J. Min. Metall. Sect. B-Metall. 54 (1) B (2018) 119 - 131

Journal of Mining and Metallurgy, Section B: Metallurgy

THERMODYNAMIC ANALYSIS OF 6XXX SERIES AL ALLOYS: PHASE FRACTION DIAGRAMS

S. Cui [a,*], R. Mishra [b], I.-H. Jung [a]

[a] Department of Mining and Materials Engineering, McGill University, Montreal, Quebec, Canada
[b] General Motors R&D Center, Warren, Michigan, USA

(Received 12 May 2017; accepted 08 December 2017)

Abstract

Microstructural evolution of 6xxx Al alloys during various metallurgical processes was analyzed using accurate thermodynamic database. Phase fractions of all the possible precipitate phases which can form in the as-cast and equilibrium states of the Al-Mg-Si-Cu-Fe-Mn-Cr alloys were calculated over the technically useful composition range. The influence of minor elements such as Cu, Fe, Mn, and Cr on the amount of each type of precipitate in the as-cast and equilibrium conditions were analyzed. Phase fraction diagrams at 500 °C were mapped in the composition range of 0-1.1 wt.% Mg and 0-0.7 wt.% Si to investigate the as-homogenized microstructure. In addition, phase fraction diagram of Mg_2Si at 177 °C was mapped to understand the microstructure after final annealing of 6xxx Al alloy. Based on the calculated diagrams, the design strategy of 6xxx Al alloy to produce highest strength due to Mg_2Si is discussed.

Keywords: *Aluminum alloy; Thermodynamic calculation; Solidification; Alloy design*

1. Introduction

Al alloys are widely used as the structural part in transportation sector due to their attractive properties, such as high strength, good corrosion resistance, formability, weldability, and low cost. Because of the continuous demands for weight reduction and improvement of fuel efficiency of automobiles, high strength Al extruded profiles of complex shape are needed in the transportation industry. 6xxx Al alloys, particularly 6063, are widely used for extrusion components in the automotive industry.

In 6xxx Al alloys, Mg and Si are the major alloying elements which trigger the formation of Mg_2Si for low temperature age-hardening [1]. In general, Si can increase the fluidity in the molten state and further the castability, improve the abrasion resistance (hard Si particles), reduce the thermal expansion coefficient, but decrease the machinability [1, 2]. Mg can improve the corrosion resistance and weldability [2]. Cu has appreciable solubility and strengthening effect [1-3]. The addition of Cu in 6xxx Al alloys can produce substantial solution and precipitation strengthening effects by forming Al_2Cu, Al_2CuMg, and Q ($Al_3Cu_2Mg_9Si_7$), improve the machinability, but decrease the corrosion resistance. Cu may also have effect on the fluidity [4].

The as-cast billet of 6xxx series Al alloys cannot always satisfy the subsequent extrusion process due to the harmful precipitates formed during casting. For instance, the size and distribution of Mg_2Si critically determine the extrusion speed, and the grain boundary particles determine the surface finish [5]. Fe impurity forms Fe-bearing intermetallic phases, such as $Al_{13}Fe_4$, α_AlFeSi, β_AlFeSi, $Al_8FeMg_3Si_6$, etc., since the solubility of Fe in Al solid solution is very low. $Al_{13}Fe_4$ forms only in Al alloys with low Si content [6]. β_AlFeSi is highly faceted and poorly bonded to the matrix. This phase has brittleness and abrasive nature, and always forms at grain boundaries and interdendritic regions during casting. β_AlFeSi is claimed to cause poor ductility and severely reduces the hot workability of Al alloys during extrusion process. The α_AlFeSi phase with compact Chinese script morphology and nonfaceted interface with Al matrix can improve the ductility and extrudability of Al alloys. The α_AlFeSi phase is also known to have no pickup defect during extrusion and can improve the properties and surface finish of the final products [7]. The unfavourable β_AlFeSi phase in the commercial 6063 alloys can transform into the less detrimental α_AlFeSi by prolonged heat treatment process [8]. However, the production cost will be increased.

Suitable amounts of Cr and Mn have been used to modify the microstructure. Dispersoid phases like Al_7(Cr, Mn), Al_4(Cr, Mn), $Al_{18}Mg_3Cr_2$, and $Al_{28}Cu_4Mn_7$ [9] can form during high temperature annealing (400–

*Corresponding author: cuisenlin@gmail.com, in-ho.jung@mcgill.ca

DOI:10.2298/JMMB170512052C

550 °C), and have strong influence on the recovery, recrystallization, and growth and result in a fine grain size. However, the introduction of Mn and Cr in Al alloys containing Si can dramatically increase the amount of coarse α_Al(Fe, Mn, Cr)Si phase which induces a rapid decrease of the alloy properties [10].

The purpose of the present study is the application of the CALPHAD-type [11-15] thermodynamic database to the design of 6xxx Al alloy. So far, no accurate thermodynamic analysis has been conducted for 6xxx Al alloys. The only relevant study for the application of the CALPHAD-type of database was carried out by Sarafoglou and Haidemenopoulos [16]. They mapped the phase fractions of Mg_2Si and β_AlFeSi for the solidification microstructure. In the present study, systematic thermodynamic analysis for the effects of common alloying elements such as Cu, Fe, Mn, and Cr, on both the solidification and equilibrium precipitates in Al 6xxx alloys was carried out using the CALPHAD-type database, and optimum compositions of high strength Al 6xxx alloys due to Mg_2Si precipitation hardening were discussed considering the casting, homogenization, extrusion, and final annealing processes. This study is part of a large Integrated Computational Materials Engineering (ICME) project to develop a new high strength Al front rail for automotive applications.

2. Thermodynamic database

There are several commercial CALPHAD-type thermodynamic databases available; FactSage-FTlite (www.factsage.com), ThermoCalc-TCAL4 (www.thermocalc.com), and Pandat-PanAluminium (www.computherm.com). Although all these databases are generally applicable for Al alloy calculations, the accuracy of these databases for specific alloy design varies because of the history of each database.

In the present study, all the CALPHAD-type thermodynamic calculations were carried out using the FactSage software [17]. The thermodynamic descriptions of all the solution and stoichiometric phases related to the Al-Mg-Si-Cu-Fe-Mn-Cr system developed by the present authors were used for the thermodynamic calculations. In this database, 21 binary systems, 18 ternary systems, and one quaternary system were optimized. A detailed list of the systems optimized in the database is shown in Table 1. Other ternary and quaternary systems were treated as ideal systems（No interaction parameters for solution phases were added).

Unfortunately, there are no comprehensive experimental data for the equilibrium phase fractions or thermodynamic properties of the solid and liquid phases in multicomponent Al 6xxx alloys. However, the database can well reproduce the phase diagrams in the Al rich corner of the Al-Mg-Si-Cu system and many ternary Al containing systems. Therefore, it is believed that the database is accurate for the phases of 6xxx Al alloys interested in the present work.

In this newly developed thermodynamic database, thermodynamic descriptions of 48 solution phases and 124 compounds are available. The solution phases include liquid, fcc_A1, hcp_A3, bcc_A2, cub_A13, cbcc_A12, diamond_A4, AlCu_ε, AlCu_η, AlCu_θ, γ_L_AlCu, γ_H_AlCu, AlCuCr_ζ, AlCuCr_κ, AlMg_β, AlMg_γ, σ_H, σ_L, $Al_{12}(Mn, Cr)$, $Al_6(Mn, Cr)$, $Al_7(Mn, Cr)$, $Al_{11}(Cr, Mn)_4$, $Al_{11}(Cr, Mn)_2$, $Al_{99}(Mn, Cr)_{23}$, Laves_C14, Laves_C15, Laves_C36, AlZnMg_τ, $S_(Al, Si)_2CuMg$, Cr_5Si_3_H, Cr_5Si_3_L, γ_L_AlCr, γ_H_AlCr, $AlCr_2$, $Al_4(Cr, Mn)$, Cr_3Si, $CrSi_2$, AlCrSi_τ3, $Al_{29}Mn_{10}$, $Al_{13}Fe_4$, Al_8Fe_5_D82, bcc_B2, $(Fe, Cr)Si$, $(Fe, Cr)_5Si_3$, α_AlFeSi, β_AlFeSi, α_AlMnSi, and β_AlMnSi.

The compounds include Al_9Cu_{11}, Cu_9Si_2, $Cu_{15}Si_4$, $Cu_{19}Si_6$, $Cu_{33}Si_7$, $CuMg_2$, $Al_{30}Mg_{23}$, Mg_2Si, Cu_3Mg_2Si, $Cu_{16}Mg_6Si_7$, $Al_7Cu_3Mg_6$, $Al_5Cu_6Mg_2$, $Al_{18}Cr_2Mg_3$, $Al_{13}Cr_4Si_4$, Al_9Cr_3Si, $Al_{116}Cr_{63}Si_{21}$, Al_9Cr_3Si, Al_2Fe, Al_5Fe_2, Fe_2Si, Fe_5Si_3, FeSi, $FeSi_2$, Fe_3Si_7, Cr_3Mn_5, $Al_{92}Cu_{67}Cr_{41}$, $Al_{65}Cu_{25}Cr_{10}$, $Al_{141}Cu_{36}Cr_{23}$, $Al_{28}Cu_4Mn_7$, $Al_{11}Cu_5Mn_3$, $AlCu_3Mn_2$, $Mn_{11}Si_{19}$, MnSi, Mn_5Si_3, Mn_3Si, Mn_9Si_2, Mn_6Si, $Al_3Cu_2Mg_9Si_7$ (Q), etc.

Table 1. *Summary of the optimized systems in the thermodynamic database.*

Binaries		Ternaries		Quaternaries
Al-Cr [18]	Cu-Fe [26]	Al-Cr-Cu [34]	Al-Mn-Si [39]	Al-Cu-Mg-Si [27]
Al-Cu [19]	Cu-Mg [27]	Al-Cr-Mg [18]	Cr-Cu-Fe [24]	
Al-Fe [20]	Cu-Mn [24]	Al-Cr-Mn [22]	Cr-Fe-Si [40]	
Al-Mg [21]	Cu-Si [28]	Al-Cr-Si [25]	Cu-Fe-Mn [24]	
Al-Mn [22]	Fe-Mg [29]	Al-Cu-Mg [27]	Cu-Mg-Si [27]	
Al-Si [23]	Fe-Mn [30]	Al-Cu-Mn [35]	Fe-Mg-Si [40]	
Cr-Cu [24]	Fe-Si [31]	Al-Cu-Si [27]	Fe-Mn-Si [41]	
Cr-Fe [24]	Mg-Mn [32]	Al-Fe-Mn [36]		
Cr-Mg [18]	Mg-Si [23]	Al-Fe-Si [37]		
Cr-Mn [22]	Mn-Si [33]	Al-Mg-Mn [38]		
Cr-Si [25]		Al-Mg-Si [23]		

3. Results and discussions

Wrought heat treatable 6xxx Al alloys for extrusion applications are produced by a sequence of metallurgical processes. Cast billet ingots are normally homogenized at 450–550 ºC depending on alloy composition. Extrusion is carried out at 400–500 ºC followed by air quenching. Age-hardening is carried out at 150–200 ºC. In the present work, solidification calculations were carried out under the Scheil-Gulliver assumption: the diffusivities of alloying elements in the solid phases were assumed to be zero and in the liquid phase were assumed to be infinite. This assumption has certain rationality since the diffusivities of alloying elements in the liquid phase are several orders larger than those in the solid state. Equilibrium phase fractions of precipitates were calculated at 500 °C and 177 °C to represent the homogenization stage and final age-hardening stage, respectively.

3.1 Effect of alloying elements on the solidification microstructure

To investigate the effects of major alloying elements on the as-cast microstructure, the Scheil calculation was performed to compute the amount of each type of precipitate. In the calculation, the composition of each element was changed from the baseline alloy composition of Al 6063.

All the computed results are shown in Fig. 1. It should be noted that open symbols refer to the left vertical axis in logarithm scale, and filled symbols to the right vertical axis in linear scale. It can be seen from Fig. 1(a) that Cr can effectively induce the formation of Al_7Cr when its content is above 0.12 wt.%. Although there is a slight increase in the weight fractions of α_AlFeSi, β_AlFeSi, Mg_2Si, Si, and $Al_8FeMg_3Si_6$, and a slight decrease in the fractions of $Al_{14}Fe_3$, Al_2Cu, Al_4(Cr, Mn), $Al_{28}Cu_4Mn_7$, and Q, they are less significant. Fig. 1(b) shows the effect of Cu. The weight fractions of Cu bearing phases such as Al_2Cu, $Al_{28}Cu_4Mn_7$, and Q increase with the increasing Cu content. Since the formation of Q substantially consumes Si, the amounts of Mg_2Si and Si decrease with Cu content. Other phases like α_AlFeSi, β_AlFeSi, Al_4(Cr, Mn), $Al_8FeMg_3Si_6$, and $Al_{13}Fe_4$ show no significant difference until Cu content reaches 0.19 wt.%. As can be seen in Fig. 1(c), β_AlFeSi is forming as soon as the Fe addition to the alloy system. When the amount of β_AlFeSi reaches 0.15 wt.% (at 0.05 wt.% Fe), α_AlFeSi begins to form. It is at 0.283 wt.% α_AlFeSi (at 0.15 wt.% Fe) that the $Al_{13}Fe_4$ phase starts since Si is not available anymore . The amounts of other phases show little difference with Fe content. The change in Mg content varies the precipitates in a more complex manner. According to the calculation in Fig. 1(d), the amount of α_AlFeSi first increases and then decreases till 0.9 wt.% of Mg. The amount of $Al_{14}Fe_3$ increases till Mg content reaches 0.9 wt.% and then it starts to decrease. The amounts of β_AlFeSi, Al_4(Mn, Cr), and Si decrease as Mg content increases. On the other hand, the amounts of Al_2Cu, Mg_2Si, $Al_{28}Cu_4Mn_7$, and Q increase. The amount of $Al_8FeMg_3Si_6$ firstly decreases and then increases with increasing Mg content. According to the current calculation in Fig. 1(e), Mn has only a slight influence on the amounts of different precipitates. With the increasing Si content, the amount of $Al_{14}Fe_3$ dramatically decreases due to the increased formations of α_AlFeSi, β_AlFeSi, Q, and $Al_8FeMg_3Si_6$. However, when the Si content reaches 0.45 wt.%, the α_AlFeSi amount starts to decrease because the composition of the alloy shifts to the β_AlFeSi phase region. Other phases show little changes with Si content.

The calculated results are summarized in Table 2. In Table 2, increase of phase amount is indicated by "↑" and decrease is indicated by "↓". As discussed above, the change of phase amount is not always straightforward due to the interplay of the alloying elements for the formation of different precipitates. With the summary in Table 2, one can select the suitable alloy composition which can give the desired as-cast microstructure. The results of the as-cast microstructure for three 6xxx Al cast billets (with composition listed in Table A1 in Appendix) are summarized in Table A2 in Appendix. The overall amounts of precipitates in as-cast microstructures are well calculated using the present database.

Table 2. *Effect of alloying elements addition on the secondary phases formation during solidification.*

Phase	Mn	Cr	Fe	Cu	Mg	Si
α_AlFeSi			↑		↓	↑↓
β_AlFeSi			↑		↓	↑
$Al_{13}Fe_4$			↑		↑	↓
Al_2Cu				↑		
Al_4(Cr, Mn)						
Mg_2Si				↓	↑	
Si				↓	↓	
$Al_8FeMg_3Si_6$					↑↓	↑
Q				↑		
$Cu_4Mn_7Al_{28}$				↑		
Al_7Cr		↑				

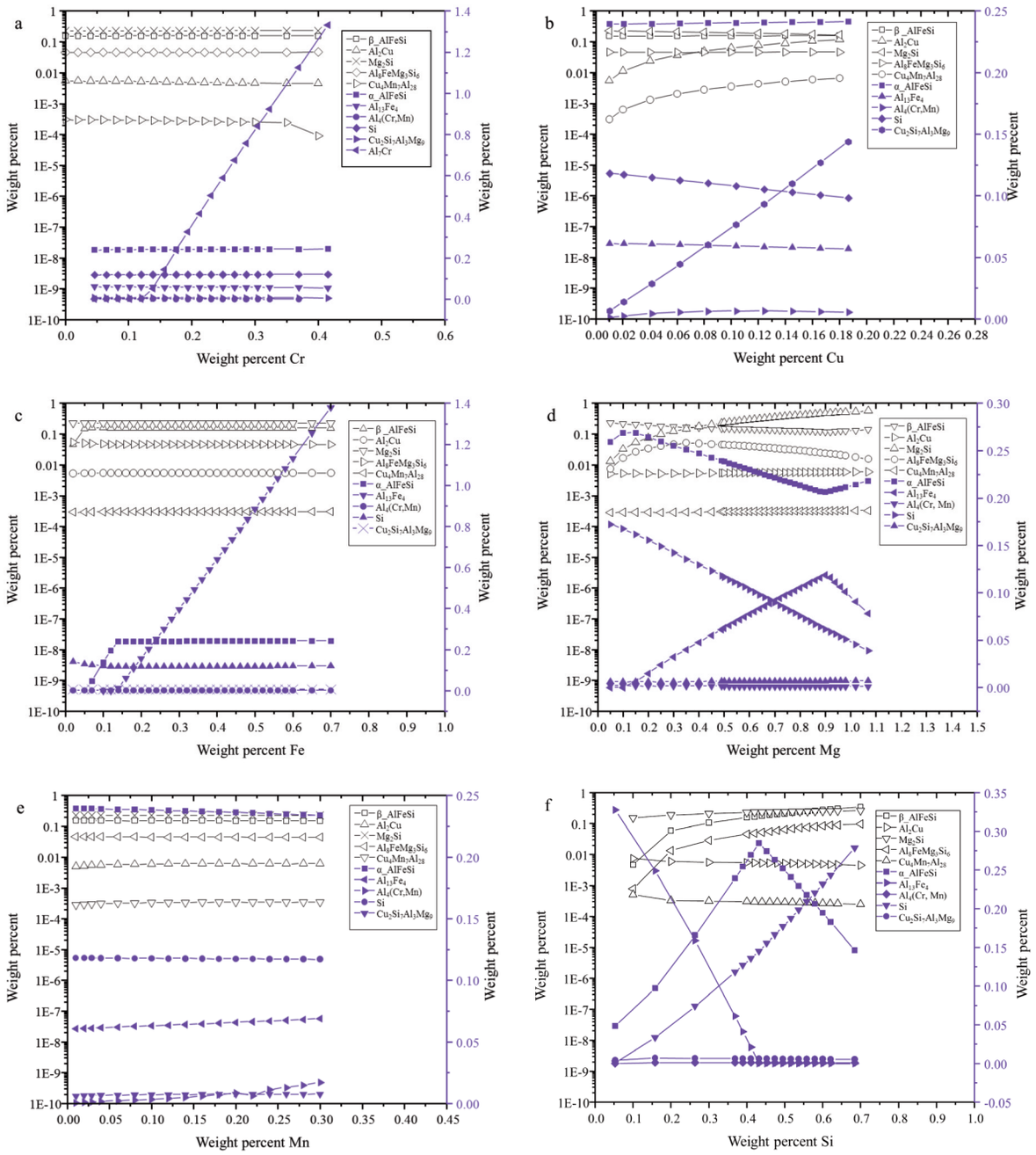

Figure 1. *Effect of alloying elements on the amounts of precipitates (secondary phases) formed during the solidification process. (a) Cr, (b) Cu, (c) Fe, (d) Mg, (e) Mn, and (f) Si.*

3.2 Equilibrium phase fraction map at 500 °C

The variation of equilibrium phase distribution of Al 6063 alloy with temperature is calculated in Fig. 2. Various precipitate phases are presented. At high temperature, $Al_{13}Fe_4$, α_AlFeSi, and β_AlFeSi are formed first. Then, $Al_{13}Fe_4$ and α_AlFeSi are dissolved into Al as temperature decreases, and $Al_8FeMg_3Si_6$ and Mg_2Si form instead. At low temperature, $Al_{12}Mn$, α_AlMnSi, and Al_2Cu are also formed. This equilibrium phase distribution calculation can give an idea for the homogenization temperature. Because the purpose of homogenization is to dissolve the precipitates and uniform the matrix composition, the material approaches the equilibrium condition. Unfortunately, there is no temperature zone

to completely dissolve all the precipitates in this case. Theoretically, to get rid of the harmful β_AlFeSi phase and minimize the precipitates, homogenization can be carried out at 590–610 °C. But this is too close to the melting temperature of Al 6063. Therefore, 460 to 500 °C can be taken as the homogenization temperature to reduce the amounts of precipitates in the as-cast microstructure. The amount of total precipitates of Al 6063 alloy (with a nominal composition listed in appendix Table A1) in the as cast microstructure is calculated to be about 0.86 wt.% as listed in appendix (see Table A2). This can be further reduced in the homogenization treatment. The suitable extrusion temperature should be lower than the homogenization temperature. The required condition of Al alloy for extrusion includes relatively low precipitate amounts (particularly, β_AlFeSi) and high temperature for a fast diffusion of the alloying elements. In this case, it can be between 450 and 500 °C.

In the current work, equilibrium phase fractions of precipitate phases at 500 °C (the possible homogenization or extrusion temperature) were mapped in the composition range of 0-0.7 wt.% Si and 0-1.1 wt.% Mg. The effects of Cu, Fe, Mn, and Cr on the precipitate amounts were also investigated. Fig. 3(a) presents the calculated phase diagram of the Al-Mg-Si alloy with 0.05 wt.% Cu, 0.15 wt.% Fe, and 0.03 wt.% Mn at 500 °C. The equilibrium phases at a given composition can be directly read from the diagram. The stable phase region of each equilibrium phase can be defined by its zero phase fraction lines. Based on this concept, the phase diagram can be divided into 5 parts, as shown in Fig. 3(b). The red line to the up-right corner of the diagram, named region 1, is the Mg_2Si formation region. The green line to the top of the diagram, named region 2, is where $Al_8FeMg_3Si_6$ forms. Above the blue line is the β_AlFeSi phase formation region, named region 3. The α_AlFeSi phase is only stable between the two orange lines (region 4), and the $Al_{14}Fe_3$ phase forms below the black line (named region 5). In the present study, the phase fraction of each precipitate was calculated based on the five phase areas.

Four series of phase fraction maps were calculated at 500 °C to show the effects of Cr, Cu, Fe, and Mn on the phase fraction of each precipitate phase. Fig. 4 shows the effect of Cr on the different precipitate phases. The Cr concentrations of 0.02 wt.% and 0.20 wt.% were selected in the calculations, and the concentrations of Cu, Fe, and Mn were fixed at 0.05, 0.15, and 0.03 wt.%, respectively. The amount of $Al_{13}Fe_4$ decreases as Si content increases. The amount of $Al_8FeMg_3Si_6$ increases as the Si content increases. At constant Si content, $Al_8FeMg_3Si_6$ shows maximum amount at around 0.8 wt.% Mg. Mg_2Si increases when both the Mg and Si contents increase. The amount of α_AlFeSi firstly increases as Si content increases and then decreases with Si content. The amount of β_AlFeSi in region 3 increases with the increasing Si content, but when region 3 is overlapping with region 2, the amount of β_AlFeSi keeps decreasing

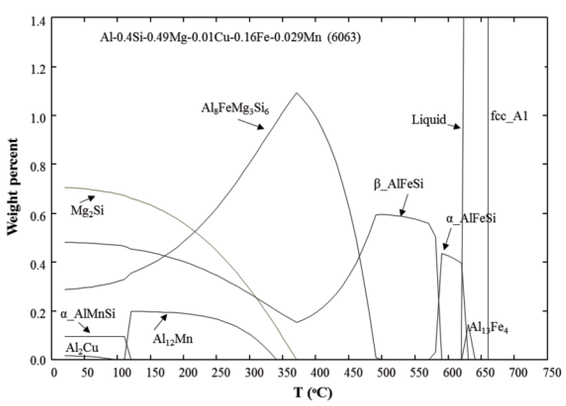

Figure 2. *Calculated equilibrium phase distribution of 6063 alloy as a function of temperature.*

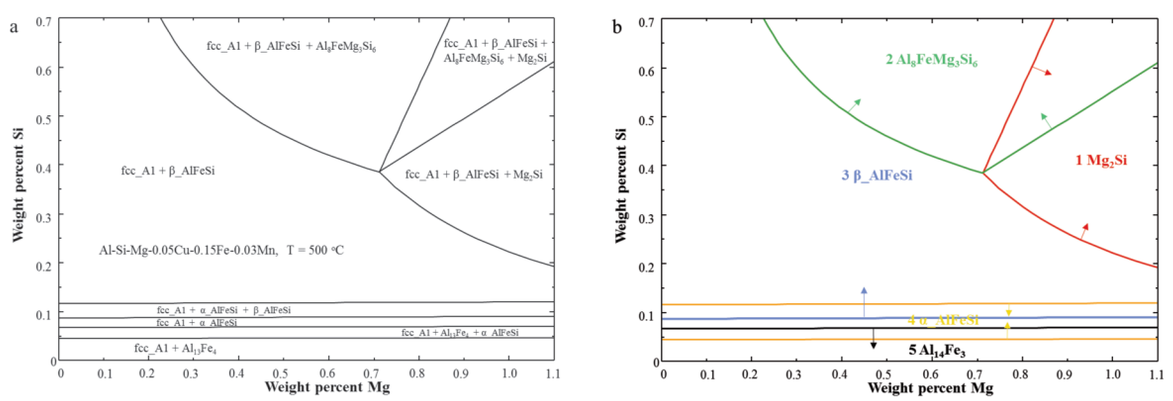

Figure 3. *(a) Calculated phase diagram of the Al-Mg-Si alloys with 0.05 wt.% Cu, 0.15 wt.% Fe, and 0.03 wt.% Mn at 500 °C, (b) the stability region of each equilibrium phase.*

due to the formation of $Al_8FeMg_3Si_6$. As shown in Fig. 4, Cr can effectively decrease the amount of $Al_{13}Fe_4$ and increase the amounts of Mg_2Si and $Al_8FeMg_3Si_6$. Besides, Cr can increase the amount of α_AlFeSi in the low Si region and decrease in the high Si region. The amount of β_AlFeSi will increase with Cr except for the part overlapped with region 2. Besides, the addition of Cr can induce the precipitation of Al_7Cr in the entire composition area as can be seen in Fig. 4(f). Fig. 5 shows the influence of Cu on the precipitates. Cu content was changed from 0.05 to 0.15 wt.%. As can be seen in the figure, Cu has nearly no influence on the precipitate amount. Fig. 6 shows the effect of Fe on the precipitates. The contents of $Al_{13}Fe_4$, α_AlFeSi, and β_AlFeSi can be substantially increased with the increasing Fe content, while that of the $Al_8FeMg_3Si_6$ phase can be decreased. As shown in

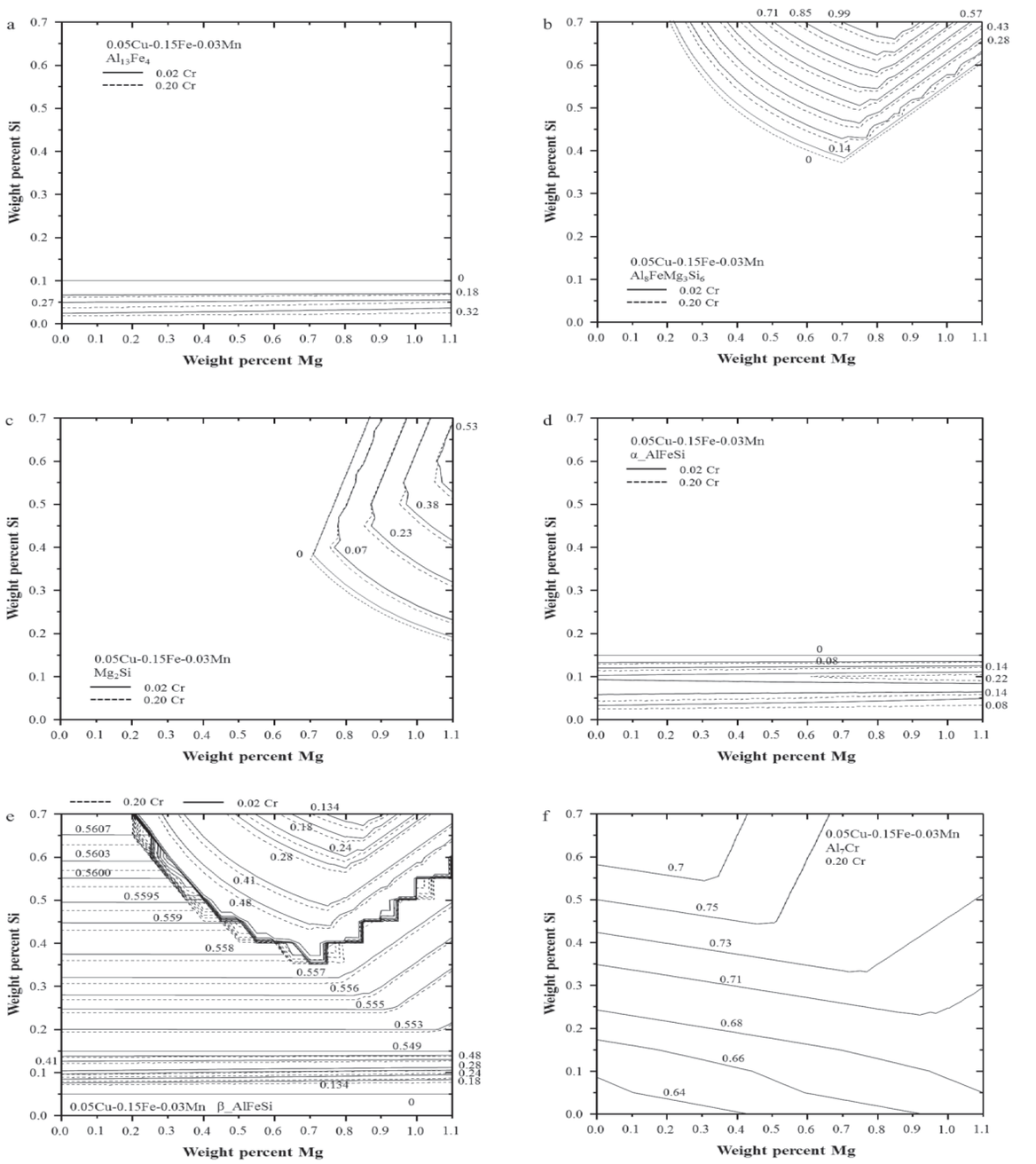

Figure 4. *Phase fraction maps (wt.%) of the (a) $Al_{13}Fe_4$, (b) $Al_8FeMg_3Si_6$, (c) Mg_2Si, (d) α_AlFeSi, (e) β_AlFeSi, and (f) Al_7Cr phases in Al-Mg-Si-0.05Cu-0.15Fe-0.03Mn with 0.02Cr or 0.20Cr at 500 °C.*

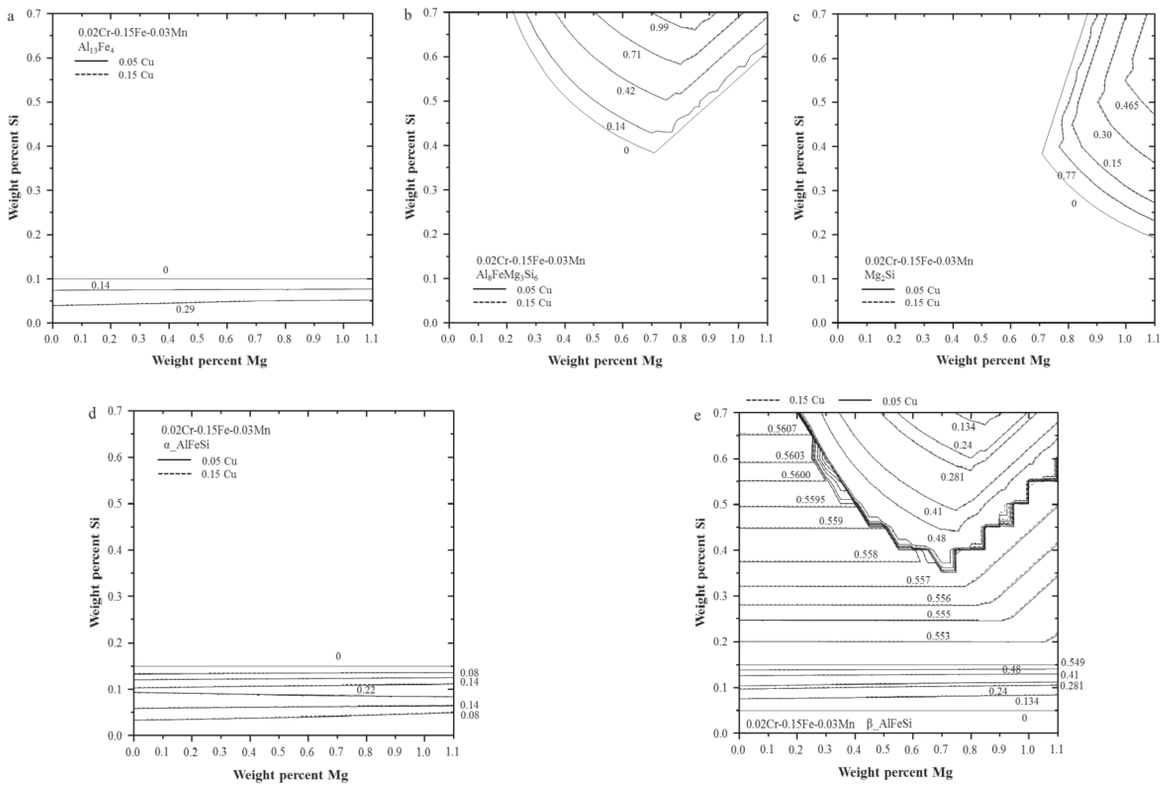

Figure 5. *Phase fraction maps (wt.%) of the (a) $Al_{13}Fe_4$, (b) $Al_8FeMg_3Si_6$, (c) Mg_2Si, (d) α_AlFeSi, and (e) β_AlFeSi phases in Al-Mg-Si-0.02Cr-0.15Fe-0.03Mn with 0.05Cu or 0.15Cu at 500 °C.*

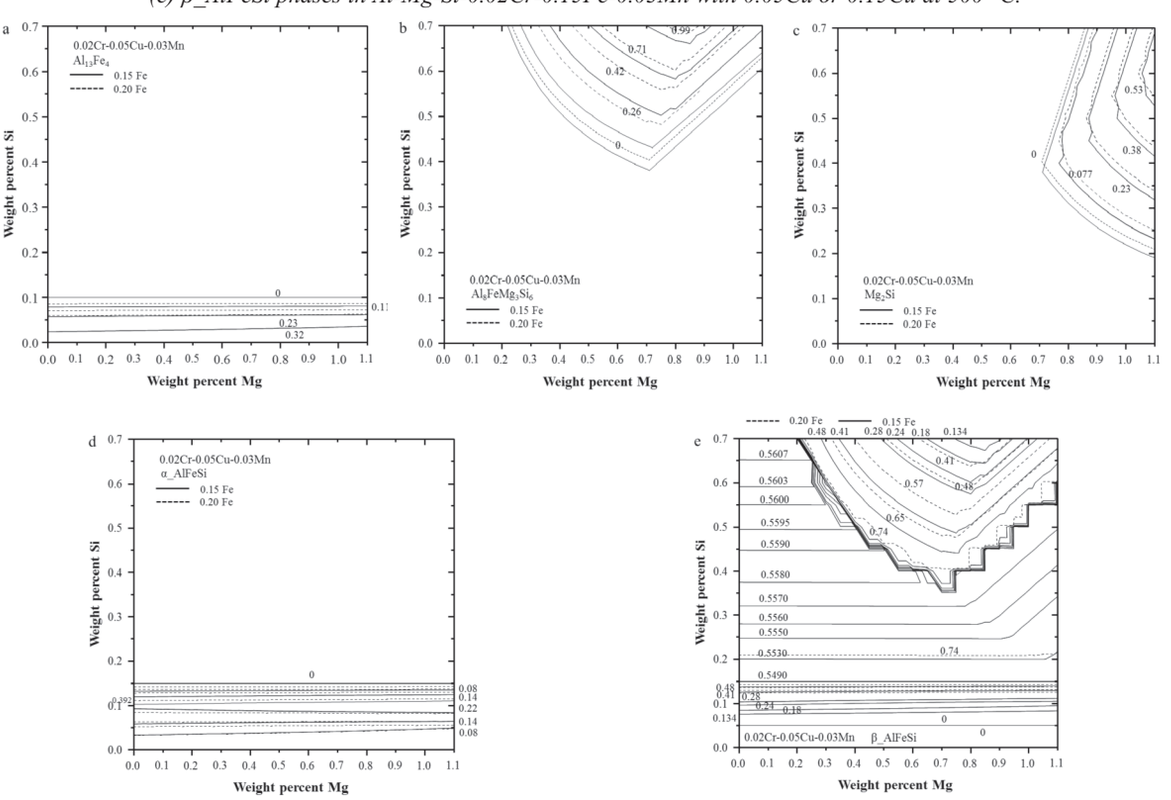

Figure 6. *Phase fraction maps (wt.%) of the (a) $Al1_3Fe_4$, (b) $Al_8FeMg_3Si_6$, (c) Mg_2Si, (d) a_AlFeSi, and (e) β_AlFeSi phases in Al-Mg-Si-0.02Cr-0.05Cu-0.03Mn with 0.15Fe or 0.20Fe at 500 °C.*

Fig. 6(c), the amount of Mg_2Si can be increased in the Si rich region and decreased in the Mg rich region. Fig. 7 compares the calculated results of 0.03 wt.% Mn with 0.1 wt.% Mn. The amounts of $Al_{13}Fe_4$, Mg_2Si, $Al_8FeMg_3Si_6$, α_AlFeSi, and β_AlFeSi change slightly but negligible with the variation of Mn. At 0.1 wt.% Mn, the $Al_{12}Mn$ phase becomes stable in the entire composition range investigated.

3.3 Discussion

From the above Scheil and equilibrium calculations, the effect of major alloying elements on the as-cast microstructure and equilibrium microstructure at homogenization and in extrusion process can be understood. This information can be very helpful in new alloy design.

In the extrusion process, for example, the amount

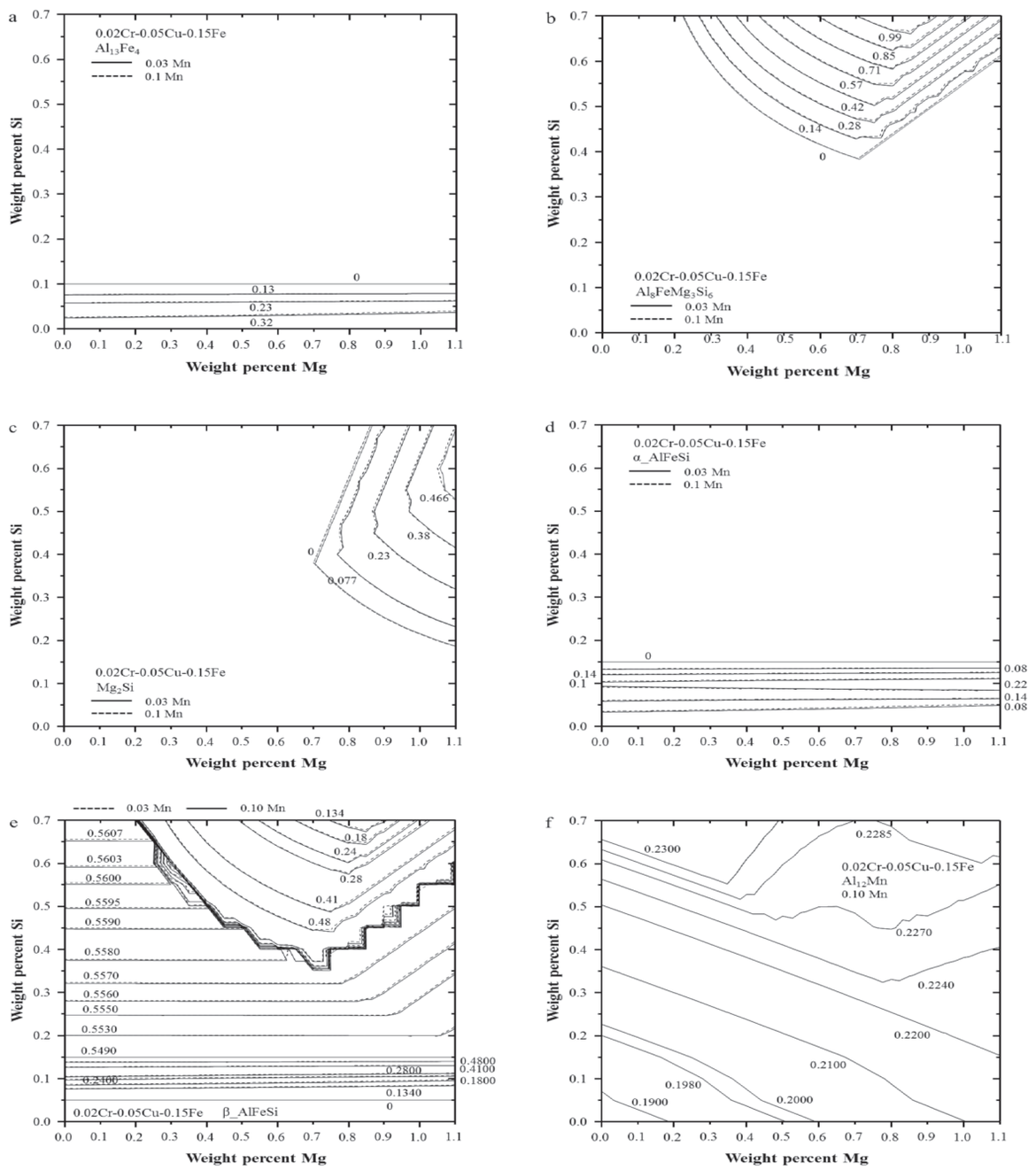

Figure 7. *Phase fraction maps (wt.%) of the (a) $Al_{13}Fe_4$, (b) $Al_8FeMg_3Si_6$, (c) Mg_2Si, (d) α_AlFeSi, (e) β_AlFeSi, and (f) $Al_{12}Mn$ phases in Al-Mg-Si-0.02Cr-0.05Cu-0.15Fe with 0.03Mn or 0.10Mn at 500 °C.*

of β_AlFeSi is considered as a major constraint due to its brittle feature. To minimize the harmful effect of β_AlFeSi, we can choose suitable alloy composition to control the as-cast and equilibrium amount of β_AlFeSi, and employ the homogenization temperature to let the β_AlFeSi transform to α_AlFeSi. According to Table 2, increasing Mg content and decreasing the contents of Si and Fe can effectively decrease the amount of β_AlFeSi in as-cast microstructure. On the other hand, the equilibrium amount of β_AlFeSi at 500 °C can be reduced by increasing Cu and decreasing Cr, Fe, Mn, and Si. An alternative way is to choose suitable homogenization procedure. As discussed before, the β_AlFeSi phase can completely transform to α_AlFeSi, if the alloy is homogenized at 590 °C for a certain time as can be seen in Fig. 2. But this may be less applicable in the real practice.

Another important issue considered in high strength 6xxx series Al alloy design is the formation of maximum amounts of metastable β' and β" phases at the age-hardening stage. However, the Gibbs energies of various metastable phases in the 6xxx series Al alloys are currently not implemented. Instead of calculating the amounts of metastable β' and β" phases directly, the present work studies the possible formation of Mg_2Si. The equilibrium amount of Mg_2Si can be an indicator of the ability of precipitation hardening by the metastable β' and β" phases which can be transformed to Mg_2Si by prolonged heat treatment. The Mg_2Si phase already formed before final heat treatment cannot be effective for precipitation hardening. Therefore, the difference of Mg_2Si amount between the heat treatment temperature and extrusion/homogenization temperature can be a useful indicator for the precipitation hardening ability. In the present study, 177 °C, which is the typical ageing temperature of Al 6063 alloys, was used for calculation. The equilibrium amount of Mg_2Si in Al-Mg-Si alloys with 0.02 wt.% Cr, 0.05 wt.% Cu, 0.15 wt.% Fe, and 0.03 wt.% Mn at 177 °C is calculated in Fig. 8. According to the calculated results, the Mg_2Si phase has its maximum amount along the Mg/Si weight ratio of 1.731:1. Addition of Mg cannot increase the amount of Mg_2Si, and the addition of Si can decrease the amount of Mg_2Si formation. The red line indicates the limit composition for the Mg_2Si formation at 500 °C, and the green line indicates the zero phase fraction line of $Al_8FeMg_3Si_6$ at 500 °C where the β_AlFeSi phase fraction begins to decrease rapidly. The green colored rectangle indicates the alloy composition range of commercial 6063 alloy, which is close to the Mg/Si ratio of 1.731:1. Even though there will be a certain amount of Mg_2Si (<0.47 wt.%) formation at the homogenization temperature in the composition range, the ability of precipitation hardening is still not significantly decreased. Whent he Mg/Si ratio changes to 1:1, which contains excess amount of Si, the ability of Mg_2Si formation shows a certain decrease compared to Mg/Si ratio of 1.731:1 at 177 °C. However, as there is no Mg_2Si formation along the 1:1 ratio line at 500 °C, Al alloy with Mg/Si ratio of 1:1 can still produce a large amount of β' and β" precipitation hardening phases as indicated by Gupta et al. [42].

Considering the minimization of the β_AlFeSi phase, reasonably low amount of the $Al_8FeMg_3Si_6$ phase at extrusion/homogenization temperature (500 °C), and maximum amount of precipitation hardening ability at 177 °C, the most optimum alloy composition range can be suggested as shown in the hatched area in Fig. 8. Of course, the annealing time for the maximum precipitation hardening should be optimized by experiment. In addition, the effect of solutes, Mg, Si, Cu, and Mn, on the extrusion flow behavior and solid solution hardening should be further considered to narrow down the alloy composition for new high strength Al 6xxx alloys. The rectangular region (composition range of commercial 6063 alloy) in Fig. 8 is very wide, and can produce quite different amount of Mg_2Si, which can significantly change the mechanical properties of the finally products. It should be noted that the design strategy can be altered if the thermodynamic descriptions of the metastable phases are available in the database. The amount of each type of metastable phase could be directly mapped. In that case, the prediction could be more applicable.

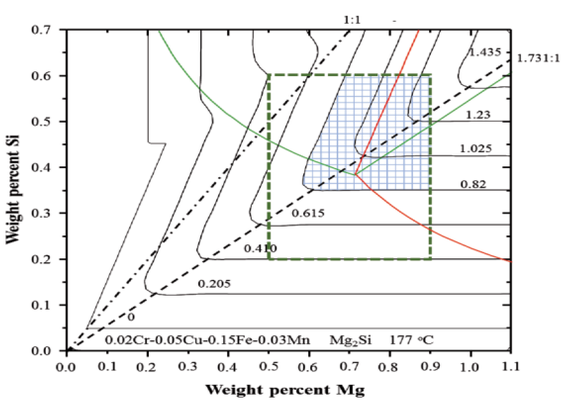

Figure 8. *Phase fraction map (wt.%) of Mg_2Si in Al-Mg-Si-0.02Cr-0.05Cu-0.15Fe-0.03Mn alloy at 177 °C.*

4. Conclusion

In the current work, a newly developed thermodynamic database for Al alloys has been used for the comprehensive thermodynamic analysis of Al 6xxx alloy development. Influence of various alloying elements such as Fe, Mn, Cu, and Cr on secondary phase formation in the Al-Mg-Si alloy was studied using Scheil cooling calculation for as-cast microstructure and equilibrium calculation for

homogenization and final heat treatment. The phase fraction maps for various precipitates were generated to show the effects of different alloying elements on the amounts of precipitate phases formed. Based on the thermodynamic analysis, the most optimum alloy composition for high strength Al 6xxx alloy is suggested for new alloy development in consideration of β_AlFeSi and precipitation hardening due to Mg_2Si. In addition, the process conditions for homogenization and extrusion are also discussed.

Acknowledgement

The authors would like to thank the financial support from NSERC-Automotive Partnership Canada program in Canada. Senlin Cui would also like to thank the McGill Engineering Doctorate Award (MEDA) from McGill University for financial support.

References

[1] P. Mukhopadhyay, ISRN Metall., (2012) 165082, 165015 pp.

[2] R.S. Rana, R. Purohit, S. Das, International Journal of Scientific and Research Publications, 2 (2012) 1-7.

[3] M.N. Ervina Efzan, H.J. Kong, C.K. Kok, Adv. Mater. Res. (Durnten-Zurich, Switzerland), 845 (2014) 355-359, 356 pp.

[4] R.N. Lumley, D.R. Gunasegaram, M. Gershenzon, R.G. O'Donnell, International Heat Treatment and Surface Engineering, 4 (2010) 25-32.

[5] J. Asensio-Lozano, B. Suarez-Pena, G.F.V. Voort, Materials, 7 (2014) 4224-4242, 4219.

[6] S. Ji, W. Yang, F. Gao, D. Watson, Z. Fan, Mater. Sci. Eng., A, 564 (2013) 130-139.

[7] K.B.S. Couto, S.R. Claves, W.H. Van Geertruyden, W.Z. Misiolek, M. Goncalves, Mater. Sci. Technol., 21 (2005) 263-268.

[8] S. Onurlu, A. Tekin, . J. Mater. Sci., 29 (1994) 1652-1655.

[9] J. Davis, Alloying: Understanding the Basics., (2001) p351-416.

[10] Y. Han, K. Ma, L. Li, W. Chen, H. Nagaumi, Mater. Des., 39 (2012) 418-424.

[11] G. Huang, L. Liu, L. Zhang, Z. Jin, J. Min. Metall. Sect. B Metall., 52 (2016) 177-183.

[12] B. Hu, B. Yao, J. Wang, J.R. Zhao, F.F. Min, Y. Du, J. Min. Metall. Sect. B Metall., 53 (2017) 95-106.

[13] J. Zhou, L. Zhang, L. Chen, Y. Du, Z.K. Liu, J. Min. Metall. Sect. B Metall., 53 (2017) 85-93.

[14] S.L. Cui, L.J. Zhang, W.B. Zhang, Y. Du, H.H. Xu, J. Min. Metall., Sect. B, 48 (2012) 227-249.

[15] S. Cui, Y. Du, L. Zhang, Y. Liu, H. Xu, Calphad, 34 (2010) 446-451.

[16] P.I. Sarafoglou, G.N. Haidemenopoulos, Int. J. Mater. Res., 105 (2014) 1202-1209.

[17] C.W. Bale, E. Belisle, P. Chartrand, S.A. Decterov, G. Eriksson, A.E. Gheribi, K. Hack, I.H. Jung, Y.B. Kang, J. Melancon, A.D. Pelton, S. Petersen, C. Robelin, J. Sangster, P. Spencer, M.A. Van Ende, CALPHAD, 55 (2016) 1-19.

[18] S. Cui, I.-H. Jung, J. Kim, J. Xin, J. Alloys Compd., 698 (2017) 1038-1057.

[19] N. Saunders, Cost 507 - Thermochemical database for light metal alloys, 2 (1991) 28-33.

[20] A.T. Phan, M.-K. Paek, Y.-B. Kang, Acta Mater., 79 (2014) 1-15.

[21] P. Chartrand, Unpublished work.

[22] S. Cui, I.-H. Jung, Metall. Mater. Trans. A, 48 (2017) 1383-1401.

[23] J.-P. Harvey, Master's thesis, Ecole Polytechnique, (2006).

[24] S. Cui, I.-H. Jung, CALPHAD, 56 (2017) 241-259.

[25] S. Cui, I.-H. Jung, J. Alloys Compd., 708 (2017) 887-902.

[26] K. Shubhank, Y.-B. Kang, CALPHAD, 45 (2014) 127-137.

[27] S. Cui, I.-H. Jung, CALPHAD, 57 (2017) 1-27.

[28] D.H. Kang, I.-H. Jung, Unpublished work.

[29] P. Chartrand, Upblished work.

[30] M.-K. Paek, Unpublished work.

[31] S. Cui, I.-H. Jung, CALPHAD, 56 (2017) 108-125.

[32] Y.-B. Kang, A.D. Pelton, P. Chartrand, P. Spencer, C.D. Fuerst, Metall. Mater. Trans. A, 38A (2007) 1231-1243.

[33] M.-K. Paek, J.-J. Pak, Y.-B. Kang, CALPHAD, 46 (2014) 92-102.

[34] S. Cui, Unpublished work.

[35] S. Cui, Unpublished work.

[36] M.-S. Kim, Y.-B. Kang, J. Phase Equilib. Diffus., 36 (2015) 453-470.

[37] M.-K. Paek, Unpublished work.

[38] A. Shukla, A.D. Pelton, J. Phase Equilib. Diffus., 30 (2009) 28-39.

[39] M.-K. Paek, Unpublished work.

[40] S. Cui, I.-H. Jung, Metall. Mater. Trans. A, 48 (2017) 4342-4355.

[41] M.-K. Paek, Unpublished work.

[42] A.K. Gupta, D.J. Lloyd, S.A. Court, Mater. Sci. Eng., A, A316 (2001) 11-17.

Appendix: Casting microstructure of Al 6xxx series alloys

As part of the present study, four billet cast alloys were analyzed and compared to the present thermodynamic calculations. Four Al alloys with their nominal compositions are listed in Table A1. The main difference of the three new Al alloys from the original Al 6063 is the addition of Cr for Al_7Cr formation, change in Mg for Mg_2Si formation, and Cu for Al_2Cu formation. Billet casting (Sapa, Canada) was performed to prepare as cast billet. The diameter of the billet was 200 mm and the cooling rate was 20 K/s. The billet was cut perpendicular to the casting direction. Specimen with a size of one cubic centimeter was cut at the half diameter distance from the surface to the center of the billet, grounded with SiC papers, and then polished with 3 μm and 1 μm

Table A1. *Alloy compositions of as-cast billets.*

Alloy	Al	Si	Mg	Cu	Fe	Cr	Mn
6063	Bal.	0.4	0.49	0.01	0.16	0	0.029
#1	Bal.	0.4807	0.4965	0.1480	0.1951	0.1820	0.0965
#2	Bal.	0.5639	0.9118	0.1351	0.2011	0	0.0950
#3	Bal.	0.5921	0.9171	0.1437	0.1987	0.1974	0.0957

diamond paste. All the intermetallic phases were characterized using scanning electron microscopy (SEM) and energy dispersive X-ray spectroscopy (EDS) analysis. The volume fractions of the precipitates were measured by image analysis software ImageJ (https://imagej.nih.gov/ij).

The calculated solidification path of the typical 6063 alloy is presented in Fig. A1(a). As can be seen from the diagram, the precipitation sequence is fcc_A1 → $Al_{14}Fe_3$ → α_AlFeSi → β_AlFeSi → Mg_2Si → $Al_8FeMg_3Si_6$ (π) → Si → Q. Solidification starts at 654 °C and ends at 512 °C. The mass of the precipitate phase as a function of the total mass percent of solid (that is, the degree of the completion of solidification) is shown in Fig. A1(b). The $Al_{14}Fe_3$ phase begins to form at 89.7 percent of solidification and reaches its maximum at 91.2 percent of solidification when the α_AlFeSi phase begins to form. At 99.4 percent of solidification, β_AlFeSi starts to form. Following the formation of β_AlFeSi, Mg_2Si, $Al_8FeMg_3Si_6$, and Si form, and finish at the final eutectic reaction temperature 512 °C. The final eutectic reaction is L = fcc_A1 + Al_2Cu + Si + $Al_8FeMg_3Si_6$ + Q.

The calculated phase fractions in the as-cast microstructure of all four alloys are listed in Table A2. It is obvious that the precipitates cannot form if

Table A2. *Calculated phase amounts from Scheil cooling calculations (wt.%).*

Phase	6063	Alloy 1	Alloy 2	Alloy 3
fcc_A1	99.138	98.024	98.527	97.583
Al_7Cr	0	0.77332	0	0.91285
α_AlFeSi	0.23934	0.30383	0.32405	0.34757
β_AlFeSi	0.15525	0.20186	0.20305	0.21898
Al_2Cu	0.00548	0.09840	0.09440	0.09910
$Al_{13}Fe_4$	0.06130	0.05880	0.06000	0.02310
Al_4(Cr, Mn)	0.00135	0.01750	0.02310	0.01410
Mg_2Si	0.22844	0.19796	0.48494	0.49531
Si	0.11812	0.13921	0.11360	0.12526
Q	0.00661	0.11858	0.11378	0.11946
$Al_8FeMg_3Si_6$	0.04600	0.06110	0.05070	0.05590
$Cu_4Mn_7Al_{28}$	0.000304	0.00546	0.00524	0.00550

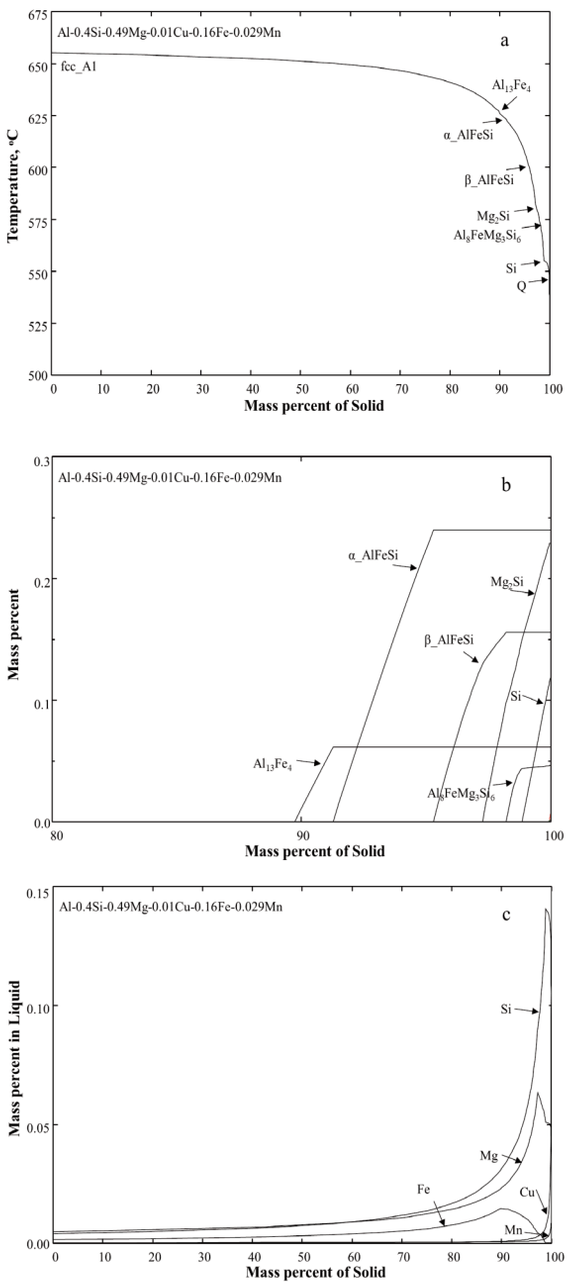

Figure A1. *(a) Calculated solidification path of 6063 alloy, (b) calculated phase fraction, and (c) calculated micro-segregation of alloying elements in the liquid phase.*

there is no segregation in the liquid phase during solidification. The calculated liquid composition as a function of solidification is shown in Fig. A1(c). The compositions of Mg, Si, and Fe show strong segregation in the liquid phase during the solidification process. It can be seen from the diagram that all the other precipitates except for the fcc_A1 phase only start to form when solidification reaches almost 90 percent where the liquid phase is enriched with Mg, Si, and Fe.

Similar to the 6063 alloy, the simulated solidification paths of the three as-cast alloys are presented in Fig. A2. The precipitation sequences of these three alloys are quite similar. The Cr containing alloys (Alloys 1 and 3) show Al_7Cr formation before the fcc_A1 phase. As shown in Table A2, the amounts of Q, Al_2Cu, and Mg_2Si in the three alloys are calculated apparently higher than those of 6063 alloy.

Fig. A3 shows the microstructure of the three cast alloys. Fig. A3(a) is the back scattered electron (BSE) micrograph of alloy 1. The Chinese script shaped α_AlFeSi, very narrow needle like β_AlFeSi, and spherical shaped Q phase were detected. Similar microstructure can be seen in Fig. A3(b) and Fig. A3(c) for alloys 2 and 3, respectively. It worth noting that the $Al_8FeMg_3Si_6$ particle with the similar shape as the Q phase was also observed in alloy 3. Other phases were not marked since the particles are very small. The primary Al_7Cr phase was not clearly observed in the micrograph shown in Fig. A3. However, a lot of fine particles rich in Cr were detected in the Al matrix in the enlarged image of alloy 1 (Fig. A3(d)). The precipitates excerpt α_AlFeSi, β_AlFeSi, and Q were not detected under SEM in the present study. Most probably, the size of the precipitates is too fine to be detected. The α_AlFeSi phase has a composition of about Al–(9.5–14.7) wt.% Fe–(5.2–10) wt.%Si, and β_AlFeSi is Al–(21.9–23.9) wt.% Fe–(7.1–9.8) wt.% Si. ImagJ software was utilized to analyze the area fraction of the precipitates in Figs. A3(a) to (c). A large area is considered during the image analysis to give a reasonable representation of the microstructure. Since it was difficult to separate the bright phases α_AlFeSi, β_AlFeSi, and Q, a total area of precipitates was measured. The volume fraction was calculated from the area fraction assuming particles are spherical. The measured total volume fractions of Q, $Al_8FeMg_3Si_6$, α_AlFeSi, and β_AlFeSi are listed in Table A3 compared with the Scheil simulation results. In the Scheil simulation results, only Q, $Al_8FeMg_3Si_6$, α_AlFeSi, and β_AlFeSi were computed for comparison. Molar volumes of all the phases were assumed to be the same. It can be seen from Table A3 that the experimental values are quite close to the simulated results. It should be noted that the Scheil calculation always overestimates the amounts of precipitates than reality due to its extreme assumptions. And the measured total volume of precipitates as listed in Table A3 also have considerable experimental errors. This is because the number of sections measured is insufficient and the measurement method itself is not advance enough. But, it can be concluded that the present simulation results are reasonable.

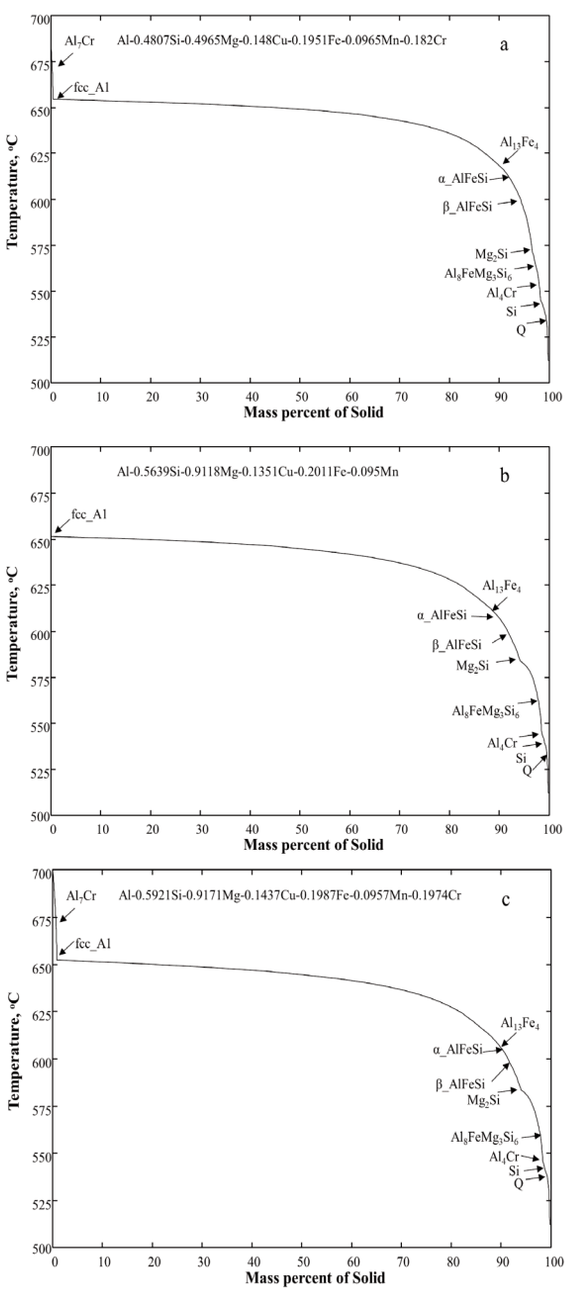

Figure A2. *Simulated solidification paths of (a) alloy 1, (b) alloy 2, and (c) alloy 3.*

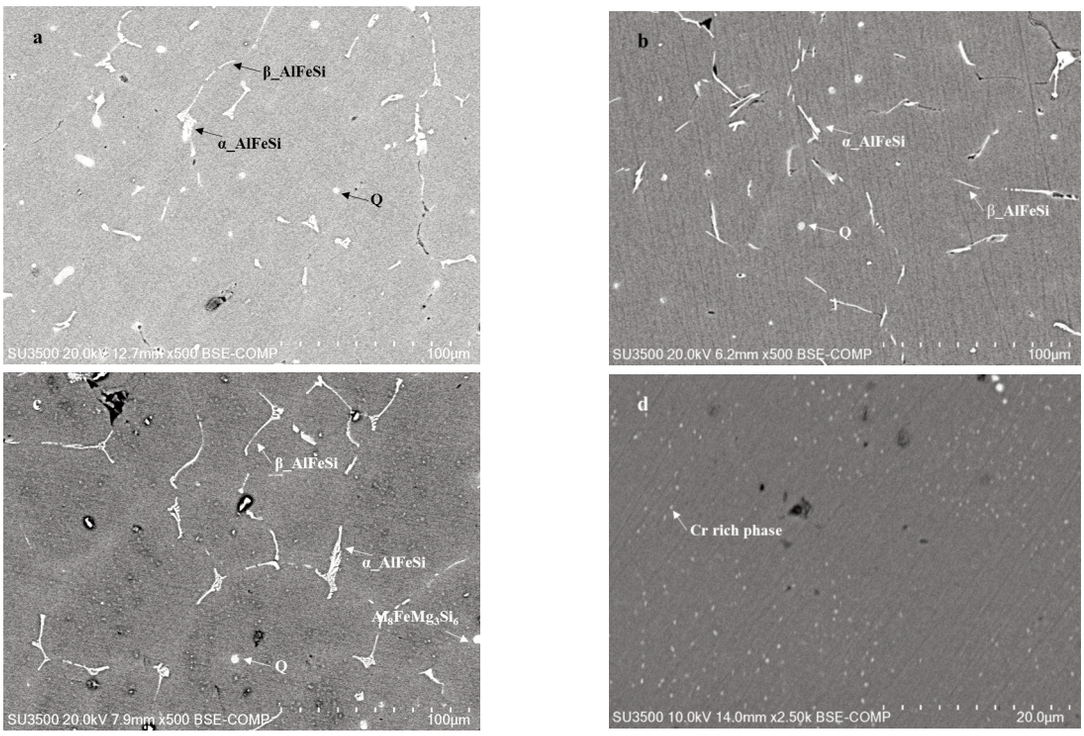

Figure A3. *Back scattered electron micrographs of (a) alloy 1, (b) alloy 2, (c) alloy 3, and (d) enlarged part of alloy 1.*

Table A3. *Total volume fractions of the Q, $Al_8FeMg_3Si_6$, α_AlFeSi, and β_AlFeSi phases from experiments compared with the calculated results.*

Alloy	measured	calculated
#1	0.00506	0.00744
#2	0.00662	0.00752
#3	0.00686	0.00765

TERMODINAMIČKA ANALIZA 6XXX SERIJE LEGURA ALUMINIJUMA: DIJAGRAMI KOLIČINA FAZE

S. Cui [a,*], R. Mishra [b], I.-H. Jung [a]

[a] Odsek za rudarstvo i materijale, Univerzitet McGill, Montreal, Kvebek, Kanada
[b] General Motors R & D Centar, Varen, Mičigen, SAD

Apstrakt

Mikrostrukturna evolucija 6xxx legura aluminijuma, tokom različitih metalurških procesa, analizirana je pomoću tačnih termodinamičkih baza podataka. Količina faza svih percipitacija koje se mogu formirati u livenom stanju, kao i u stanju ravnoteže Al-Mg-Si-Cu-Fe-Mn-Cr legura, izračunati su u tehnički iskoristivom sastavu. Analiziran je uticaj manje sadrživih elemenata, kao što su Cu, Fe, Mn i Cr, na količinu svake percipitacije u livenom i stanju ravnoteže. Dijagrami količine faze na 500°C su obeleženi u sastavu koji je sadržao 0-1.1 wt.% Mg i 0-0.7 wt.% Si da bi se ispitala tako dobijena homogenizovana mikrostruktura. Pored toga, dijagram količine faze Mg_2Si na 177 °C je obeležen radi lakšeg razumevanja mikrostrukture nakon finalnog kaljenja 6xxx legure aluminijuma. Na osnovu dobijenih dijagrama, razmatrana je strategija za proizvodnju najčvršće 6xxx legure aluminijuma u odnosu na Mg_2Si.

Ključne reči: *Legura aluminijuma; Termodinamički proračuni; Očvršćivanje; Sastav legure.*